

Exploratory Study of Transverse Proximity Effect around BAL Quasars

TORU MISAWA,¹ RIKAKO ISHIMOTO,² SATOSHI KOBU,³ NOBUNARI KASHIKAWA,^{2,4} KATSUYA OKOSHI,⁵
AKATOKI NOBORIGUCHI,¹ MALTE SCHRAMM,⁶ AND QIANG LIU³

¹*School of General Education, Shinshu University, 3-1-1 Asahi, Matsumoto, Nagano 390-8621, Japan*

²*Department of Astronomy, Graduate School of Science, The University of Tokyo, 7-3-1 Hongo, Bunkyo, Tokyo 113-0033, Japan*

³*Department of Physics, Faculty of Science, Shinshu University, 3-1-1 Asahi, Matsumoto, Nagano 390-8621, Japan*

⁴*Research Center for the Early Universe, The University of Tokyo, 7-3-1 Hongo, Bunkyo-ku, Tokyo 113-0033, Japan*

⁵*Institute of Arts and Sciences, Tokyo University of Science, 6-3-1, Niijyuku, Katsushika, Tokyo 125-8585, Japan*

⁶*Graduate school of Science and Engineering, Saitama Univ. 255 Shimo-Okubo, Sakura-ku, Saitama City, Saitama 338-8570, Japan*

ABSTRACT

We aim to find out the reason why there exists an anisotropic H I absorption around quasars; i.e., the environments around quasars are highly biased toward producing strong H I absorption in transverse direction while there exists a significant deficit of H I absorption within a few Mpc of quasars along line-of-sight. The most plausible explanation for this opposite trend is that the transverse direction is shadowed from the quasar UV radiation due to dust torus. However, a critical weakness of this idea is that we have no information on inclination angle of our sightline relative to the torus. In this study, we examine environments of quasars with broad absorption troughs in their spectra (i.e., BAL quasars) because it is widely believed that BAL troughs are observed if the central continuum is viewed from the side through their powerful outflows near the dust torus. With closely separated 12 projected quasar pairs at different redshift with separation angle of $\theta < 120''$, we examine H I absorption at foreground BAL quasars in spectra of background quasars. We confirm there exist optically thick gas around two of 12 BAL quasars, and that the mean H I absorption strength is $EW_{\text{rest}} \sim 1\text{\AA}$. These are consistent to the past results around non-BAL quasars, although not statistically significant. However, the origins of optically thick H I absorbers around BAL and non-BAL quasars could be different since their column densities are different by ~ 3 orders of magnitude. The larger sample would be required for narrowing down possible scenarios for the anisotropic H I absorption around quasars.

Keywords: Broad-absorption line quasar (183) — Quasar absorption line spectroscopy (1317) — Inter-galactic medium (813)

1. INTRODUCTION

Quasars have potential to influence the evolution of their host galaxies as well as their environments by ejection of mass, energy, and angular momentum through outflowing winds and energetic radiation from accretion disks (i.e., feedback effect). The radiation effect has been partially confirmed as the relative lack of H I absorbers in circum-galactic medium (CGM) and intergalactic medium (IGM) in the vicinity of quasars along the line of sight within a few Mpc of the quasar redshift, produced by the enhancement of local radiation field by

quasars (known as Line-of-sight Proximity effect; LPE) (Bajtlik et al. 1988; Scott et al. 2000). Indeed, the enhancement in the radiation field by the quasar relative to the extragalactic UV background is, for example, a factor of ~ 1000 at a proper scale of 100 kpc (~ 10 at 1 Mpc) from quasars with a typical bolometric luminosity of $\log L_{\text{bol}}/(\text{ergs s}^{-1}) \sim 46$ at $z \sim 2.5$. If the quasars emit UV radiation isotropically, we should detect the same trend (i.e., a deficit in H I absorption) in *transverse* direction, too (so-called transverse proximity effect; TPE). However, the TPE has not been detected in spite of many attempts (e.g., Croft 2004 and references therein).

Hennawi et al. (2006) carried out an intensive quasar survey to examine environments around quasars in

transverse direction using quasar pairs. As a part of this “quasars probing quasars (QPQ)” project whose targets are mainly Type 1 quasars, Prochaska et al. (2013) collected 650 projected quasar pairs from SDSS/BOSS quasar catalog with physical separation of $\lesssim 1$ Mpc at $z \sim 2.5$. They revealed that i) absorption strength (i.e., rest-frame equivalent width; EW_{rest}) of H I increases monotonically with decreasing a transverse distance (R_{\perp}) from quasars by $EW_{\text{rest}} = 2.3 \text{ \AA} (R_{\perp}/100 \text{ kpc})^{-0.46}$, and ii) a detection rate of optically thick H I absorbers with $\log N_{\text{HI}}/(\text{cm}^{-2}) \geq 17.2$ is very high ($\sim 60\%$ at $R_{\perp} < 100$ kpc and $\sim 20\%$ at $R_{\perp} \simeq 1$ Mpc, respectively), while the detection rate near the quasars along the line of sight is only $\sim 5\%$, close to the random distribution. The discrepancy still remains even after correcting over density effect (Jalan et al. 2019). Thus, regions transverse to quasars exhibit *enhanced* H I absorption in contrast to the measurements along the line of sight.

This opposite trend implies that the physical condition of H I absorbers is highly anisotropic around Type 1 quasars. The most plausible explanation is that the transverse direction is shadowed from the quasar UV radiation due to obscuration effect (an anisotropic scenario; Prochaska et al. 2013; Jalan et al. 2019). An anisotropic radiation can be realized by AGN unification models where the black hole is obscured by a dust torus (e.g., Antonucci 1993; Elvis 2000). Indeed, studies of Type 2 quasars and the X-ray background suggests that quasars have $\sim 30\%$ of the solid angle obscured (Ueda et al. 2003; Treister & Urry 2005). This scenario is also supported by the negative results for detecting Ly α fluorescent emission from optically thick H I absorbers near the quasars in transverse direction whose fluorescent surface brightness exceeds the detection limit if we assume isotropic radiation (Hennawi & Prochaska 2013). Thus, the anisotropic scenario is promising, but with a single critical weakness remains; we have no information on viewing angle (i.e., inclination angle) of our sightline relative to the dust torus.

Broad absorption troughs with $\text{FWHM} \geq 2000$ km/s (i.e., broad absorption lines; BALs) are present in spectra of about 15 – 40% of optically-selected quasars (e.g., Weymann et al. 1991; Knigge et al. 2008; Allen et al. 2011). There are two possible scenarios to explain the existence of BAL features. The first one is an orientation scenario; BALs are observed if normal quasars are viewed along a particular line of sight, almost parallel to the radiatively driven equatorial outflow wind whose inclination angle relative to the rotation axis of an accretion disk is large and close to the direction of (but not fully obscured by) dust torus (e.g., Murray et al. 1995; Proga et al. 2000). The another possibility is an evo-

lution scenario; BAL quasars (especially low-ionization BALs (LoBALs) with absorption lines of low-ionization species like Mg II) could represent an early stage in the lifetime of the quasar. At this stage, an extreme starburst approaches its ends and the surrounding dust cocoon are being blown away. Indeed, a significant fraction of them are dust-reddened quasars (Farrah et al. 2007; Urrutia et al. 2009) and star formation rate depends on the existence of (Lo)BALs (Chen et al. 2022).

Prochaska et al. (2013) and Jalan et al. (2019) excluded BAL quasars from their samples. Thus, the environment around BAL quasars (i.e., our sightline is close to edge-on) is expected to be different from those around non-BAL quasars (close to face-on). Here, we emphasize that we cannot examine the LPE around BAL quasars because broad and strong BAL features prevent us from measuring H I absorption amplitude adequately near the quasars.

If we find that an H I absorption around BAL quasars in the transverse direction is weaker than those expected around non-BAL quasars, it would lead to some important results: i) quasar radiation is anisotropic as expected due to the dust torus, ii) BAL winds are driven into a generally equatorial direction (i.e., closer to dust torus) as expected, and iii) the detectability of BAL features mainly depends on our viewing angles to the BAL wind (i.e., the orientation scenario) with the evolution scenario as a secondary effect. On the other hand, if an H I absorption around BAL quasars in the transverse direction is at the same level as seen around non-BAL quasars, we can confirm that i) we always observe Type 1 quasars regardless of the existence of BAL profiles, and/or that ii) we cannot use BAL quasars as an indicator that they are being observed from a direction close to the side (i.e., the evolution scenario is more applicable to BAL features; e.g., L  pari & Terlevich 2006).

In this study, we perform the survey for BAL quasars that were excluded in the past studies. We examine the proximity effect around quasars in transverse direction using BAL quasars and compare them to non-BAL quasars from the literature, and locate the origin of the anisotropically distributed H I absorbers. We describe target selection and the observations in §2, and the data analysis in §3. The results and discussion are presented in §4 and §5. We close by summarizing our results in §6. Throughout the paper, we use a cosmology with $H_0=70$ km s $^{-1}$ Mpc $^{-1}$, $\Omega_m=0.26$, and $\Omega_\Lambda=0.74$ matching to those used in Prochaska et al. (2013).

2. SAMPLE AND OBSERVATIONS

2.1. Sample Selection

We searched the quasar catalogs of SDSS/BOSS DR16 (Lyke et al. 2020) for quasar pairs that satisfy the criteria below: 1) an emission redshift of a foreground (f/g) quasar ($z_{f/g}$) is greater than 2.0 so that we can detect H I absorption lines at observed wavelength of $\lambda_{\text{obs}} \gtrsim 3650\text{\AA}$ in SDSS/BOSS spectra of a background (b/g) quasar, 2) a separation angle between quasars is $\theta < 120''$ which corresponds to $R_{\perp} \lesssim 1$ Mpc at $z \sim 2.5$ within which the radiation from the quasar dominates the UV background (i.e., the ionization condition of the CGM and IGM strongly depends on the existence of the dust torus of a f/g quasar), 3) a BAL profile is present in the spectrum of a f/g quasar (i.e., Balnicity Index¹ (BI) > 0) while a b/g quasar has no remarkable absorption feature (i.e., BI = 0 and Absorption Index² (AI) = 0)³, 4) a radial velocity difference between f/g and b/g quasars, Δv ($z_{b/g} - z_{f/g}$), is larger than 5,000 km/s to avoid the line-of-sight proximity effect of a b/g quasar, 5) H I Ly α absorption lines at $z_{f/g}$ do not blend with Ly β or higher order Lyman series lines at $z \gtrsim z_{f/g}$ (i.e., $(1+z_{f/g}) \times 1216$ should be larger than $(1+z_{b/g}) \times 1026$), and 6) g -band magnitude of both f/g and b/g quasars are bright enough ($g \lesssim 20.0$) to acquire a high-quality spectrum.

Among 750,414 quasars in Lyke et al. (2020), we found 12 projected quasar pairs⁴ satisfying all the criteria above as listed in Table 1. Our sample quasars are well representative with respect to the global BAL quasar population, as compared in Figure 1, except that they are biased toward brighter ones (due to our selection criterion). We will refer to them as PQ1 through PQ12 according to their coordinates. Some of them have been observed more than once in the Sloan Digital Sky Survey (SDSS)-I/II/III/IV as shown in Table 2.

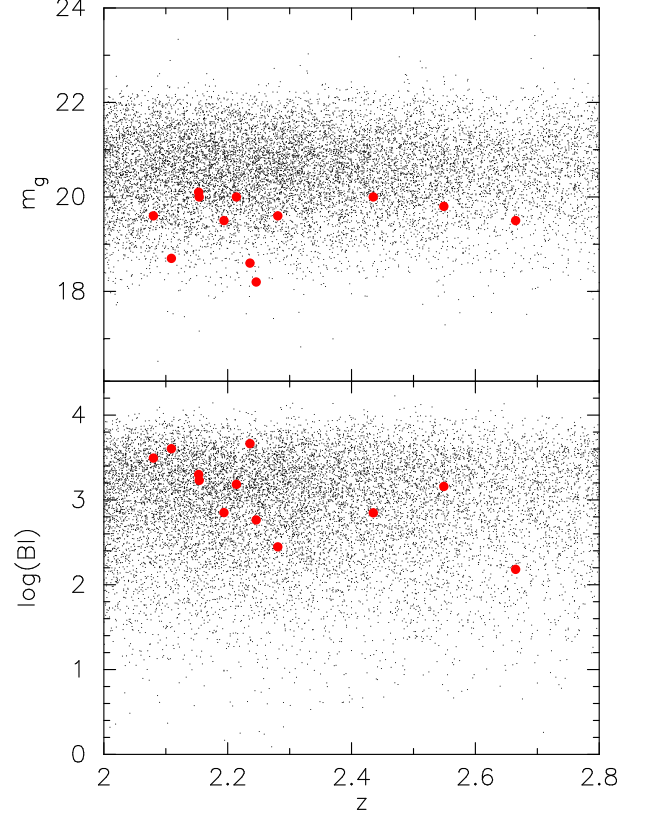


Figure 1. g -band magnitude (m_g) and Balnicity index (BI) as a function of redshift of our 12 foreground quasars (red dotted circles) and all BAL quasars (black dots) from Lyke et al. (2020). In the redshift range shown, a flux at 1325\AA in the rest-frame (which is used to estimate the specific flux in Section 3.3) is redshifted into the wavelength range of g -band filter.

2.2. Subaru/FOCAS Observations

We additionally obtained spectra of b/g quasars of 3 relatively bright quasar pairs (PQ9, PQ10, and PQ11) with Subaru/FOCAS on 2021 June 18, using a similar resolution power ($R \sim 2,000$) to those of the SDSS/BOSS spectra. These quasars have the highest redshift of f/g quasars among our sample, and two of them (PQ10 and PQ11) have strong H I absorption systems (i.e., Damped Ly α (DLA) systems) as discovered by Lyke et al. (2020).⁵ Precise measurement of their H I column density is crucial for our analysis because one of our purposes is to estimate the covering fraction of optically thick absorbers like DLAs around the BAL quasars. We observed them using a VPH450 grism with a $0''.6$ slit width under clear and stable sky conditions

¹ Balnicity Index was originally introduced by Weymann et al. (1991) as

$$BI = \int_{3000}^{25000} \left(1 - \frac{f(-v)}{0.9}\right) C dv, \quad (1)$$

where $f(-v)$ is the continuum-normalized flux at a velocity of v (in km s^{-1}) from C IV or Si IV emission-line center, C is a constant equal to 1 in regions where $f(-v)$ has been continuously less than 0.9 for at least 2000 km s^{-1} (otherwise, $C = 0$).

² Absorption Index is computed by the same equation as BI, but the integration range is slightly different as defined by Hall et al. (2002).

³ We used the values of BI and AI in Lyke et al. (2020), but we also visually checked the existence of strong absorption lines ourselves.

⁴ Before placing the final criterion on g -band magnitude, we have 337 projected quasar pairs that would be possible targets for future observations.

⁵ They are identified at $z_{\text{DLA}} = 2.539$ and 2.443 in b/g quasars of PQ10 and PQ11, respectively.

Table 1. Sample Quasars

ID	f/g or b/g	quasar	z_{em}^a	m_g	m_i	BI ^b	AI ^c	θ^d
				(mag)	(mag)	(km s ⁻¹)	(km s ⁻¹)	(arcsec)
PQ1	f/g	SDSS J003135.57+003421.2	2.236±0.003 ^e	18.6	18.4	4618	5602	62
	b/g	SDSS J003138.18+003333.2	2.741±0.004	19.2	19.0	0	0	
PQ2	f/g	SDSS J021631.70+034009.9	2.109±0.003	18.7	18.1	4017	5440	25
	b/g	SDSS J021630.65+034029.4	2.445±0.003	19.7	19.7	0	0	
PQ3	f/g	SDSS J092223.04+160531.4	2.281±0.003	19.6	19.4	280	1234	101
	b/g	SDSS J092216.04+160526.4	2.373±0.003	18.1	18.0	0	0	
PQ4	f/g	SDSS J095612.57+370052.9	2.153±0.003	20.1	19.8	1997	2458	71
	b/g	SDSS J095618.43+370106.2	2.686±0.004	20.0	19.8	0	0	
PQ5	f/g	SDSS J110532.92+515559.7	2.214±0.003	20.0	19.5	1527	2893	46
	b/g	SDSS J110529.06+515530.3	2.439±0.003	19.9	19.7	0	0	
PQ6	f/g	SDSS J123042.00+363527.6	2.194±0.003	19.5	19.4	708	1004	91
	b/g	SDSS J123049.33+363550.4	2.649±0.004	19.7	19.7	0	0	
PQ7	f/g	SDSS J124547.67+341822.6	2.080±0.003	19.6	19.2	3110	5358	73
	b/g	SDSS J124546.58+341934.8	2.593±0.004	19.9	19.7	0	0	
PQ8	f/g	SDSS J135417.90+334859.8	2.246±0.003	18.2	18.0	580	985	109
	b/g	SDSS J135414.28+334720.4	2.321±0.003	19.8	19.6	0	0	
PQ9	f/g	SDSS J144539.14+373336.0	2.665±0.004	19.5	19.4	152	489	69
	b/g	SDSS J144544.90+373328.9	2.963±0.004	19.2	19.1	0	0	
PQ10	f/g	SDSS J150723.66+255216.6	2.549±0.004	19.8	19.6	1441	2504	92
	b/g	SDSS J150717.25+255144.6	2.718±0.004	19.5	19.3	0	0	
PQ11	f/g	SDSS J224015.85+221230.2	2.435±0.003	20.0	19.8	704	2175	110
	b/g	SDSS J224013.34+221414.1	2.675±0.004	19.0	18.9	0	0	
PQ12	f/g	SDSS J233011.09+254731.1	2.154±0.003	20.0	19.3	1699	2460	93
	b/g	SDSS J233017.52+254803.0	2.297±0.003	19.2	19.1	0	0	

^aMg II-based emission redshift and its uncertainty (see Section 3.2).

^bBalnicity Index from Lyke et al. (2020).

^cAbsorption Index from Lyke et al. (2020).

^dAngular separation between projected pair quasars in arcsec.

^eEmission redshift from Filiz Ak et al. (2013).

with the typical seeing size of 0''7. The CCD was binned every 2 pixels in the both spatial and dispersion directions (i.e., $\sim 1.28\text{\AA}$ per pixel). We adopt 5 pixels as an extraction aperture. Total exposure time is 5400s, 5400s, and 8400s for b/g quasars of PQ9, PQ10, and PQ11, respectively.

We reduced the data in a standard manner with the IRAF software⁶. Wavelength calibration was performed

using the spectrum of a Th-Ar lamp. We carried out the flux calibration of the spectra using the spectrum of the spectrophotometric standard star Hz 44. The final S/N ratios of the three quasars at $\lambda_{\text{obs}} \sim 1215.67 \times (1+z_{\text{f/g}})$ are improved from those of SDSS spectra as shown in Table 2.

3. ANALYSIS

3.1. Normalization of background quasar spectra

Before measuring H I optical depth, we need to normalize spectra of b/g quasars. However, wavelength regions shorter than the Ly α emission lines are severely affected by Ly α forest, which prevents us from directly

⁶ IRAF is distributed by the National Optical Astronomy Observatories, which are operated by the Association of Universities for Research in Astronomy, Inc., under cooperative agreement with the National Science Foundation.

Table 2. Observations of b/g Quasars

Target	Obs Date (mm-dd-yyyy)	Survey/Instrument ^a	S/N ^b (pix ⁻¹)
PQ1 b/g	09-08-2010	SDSS (4220-55447-0966)	11
	12-19-2001	SDSS (0689-52262-0504)	7
	10-25-2017	SDSS (9409-58051-0509)	7
PQ2 b/g	11-06-2010	SDSS (4264-55506-0464)	6
PQ3 b/g	03-12-2012	SDSS (5307-55998-0198)	25
	03-24-2006	SDSS (2440-53818-0452)	17
	02-27-2012	SDSS (5305-55984-0944)	18
	01-30-2017	SDSS (9581-57783-0704)	21
PQ4 b/g	01-26-2011	SDSS (4573-55587-0944)	7
PQ5 b/g	04-03-2013	SDSS (6706-56385-0074)	8
PQ6 b/g	04-16-2010	SDSS (3965-55302-0060)	8
PQ7 b/g	05-06-2010	SDSS (3971-55322-0189)	6
PQ8 b/g	03-19-2010	SDSS (3861-55274-0718)	9
PQ9 b/g	04-29-2012	SDSS (5173-56046-0008)	15
	04-20-2004	SDSS (1382-53115-0607)	8
	06-18-2021	Subaru/FOCAS	22
PQ10 b/g	05-27-2012	SDSS (6019-56074-0800)	11
	06-18-2021	Subaru/FOCAS	42
PQ11 b/g	10-05-2012	SDSS (6307-56205-0418)	12
	08-30-2005	SDSS (2261-53612-0283)	11
	09-11-2012	SDSS (6119-56181-0831)	11
	06-18-2021	Subaru/FOCAS	28
PQ12 b/g	10-05-2013	SDSS (6304-56570-0848)	10

^aData source (SDSS or Subaru/FOCAS). In the case of SDSS, `plate-MJD-fiber` information is added in parenthesis.

^bSignal to noise ratio at $\lambda_{\text{obs}} \sim 1215.67 \times (1+z_{\text{f/g}})$ per pixel ($\Delta\lambda \sim 1.0\text{\AA}$ and 0.75\AA for SDSS and Subaru/FOCAS spectra, respectively). The S/N ratio is estimated not in the observed (i.e., absorbed) flux, but in the estimated continuum of the b/g quasars.

fitting the continuum level. Therefore, we estimate the continuum level of the quasar intrinsic spectra at the rest-frame wavelength of $\lambda_{\text{rest}} < 1215.67\text{\AA}$ using a principal component analysis (PCA) of low-redshift quasar spectra, following the same manner as Ishimoto et al. (2020). We fit the quasar’s spectra from the peak of Ly α emission lines up to $\lambda_{\text{rest}} \sim 1600\text{\AA}$, 2000\AA (or upper limits of the observed spectra) using 7 – 10 principal component spectra (PCS) of Suzuki et al. (2005) or Pâris et al. (2011). In Figure 2, we show the result of PCA fits to the b/g quasar of PQ4 (MJD:55587) along with the observed spectra as an example. The PCA fits moderately reproduce a global pattern of the continuum level in Ly α forest, but they over/under-estimate about half of the

observed spectra with the difference of $\lesssim 10\%$. Therefore, we manually fit a continuum level to the PCA-fit normalized spectra again, using a low-order spline function as done in Prochaska et al. (2013) and Jalan et al. (2019). Using the final spectra, we measured the mean flux levels of Ly α forest within $\pm 10000\text{ km s}^{-1}$ of the $z_{\text{f/g}}$, and confirmed that the difference between the expected (from Faucher-Giguère et al. 2008) and the observed flux levels distribute from -4.9% to $+7.8\%$ with the average of $\sim 1\%$ ⁷. Jalan et al. (2019) noticed that the manually fitted continuum level tends to be underestimated compared to the true level, especially for low-resolution spectra of quasars at higher redshift ($z > 2.6$). However, the under-estimation is almost negligible for the spectra of our targets at relatively lower redshift ($\langle z \rangle \sim 2.3$) with higher S/N ratio ($\langle \text{S/N} \rangle \sim 13\text{ pixel}^{-1}$) since the level of under-estimation has a positive (or negative) correlation with S/N ratio (or redshift), respectively (Faucher-Giguère et al. 2008). For quasars that have been observed more than once (PQ1, PQ3, PQ9, and PQ11), we apply the normalization process above for each exposure respectively and combine them to increase an S/N ratio. For PQ9, PQ10, and PQ11, we will use FOCAS and SDSS spectra separately without combining them together to avoid any possible systematic biases due to the difference in observing configurations. Normalized spectra of 12 SDSS and 3 FOCAS spectra are presented in Figures 3 and 4.

3.2. Systemic Redshift of foreground quasars

We need accurate estimation of the systemic redshift of foreground quasars for the analyses of TPE. Lyke et al. (2020) presented a primary redshift as the best estimation of systemic redshift among several methods including visual inspection, pipeline, neural network, and so on. The primary redshift of all quasars (except for the f/g quasar of PQ4⁸) are visually inspected based on the peak of the Mg II emission lines (Pâris et al. 2017). The Mg II-based redshifts are on average 57 km s^{-1} blueshifted from systemic redshifts based on stellar Ca II absorption lines (Shen et al. 2016) and their total uncertainty is $\sim 300\text{ km s}^{-1}$ (i.e., $\delta z \sim 0.003$ at $z \sim 2$) including intrinsic, systematic, and statistical errors (Shen et al. 2016; Jalan et al. 2019). We adopted the same value as the typical uncertainty of systemic redshift as shown in Table 1. Since the velocity shift of the Mg II-based

⁷ For PQ10 and PQ11, we masked spectral regions around DLA systems before measuring the flux level.

⁸ Redshift of this quasar was estimated using a pipeline in Lyke et al. (2020), but we confirm the measured redshift is consistent to the emission redshift of Mg II.

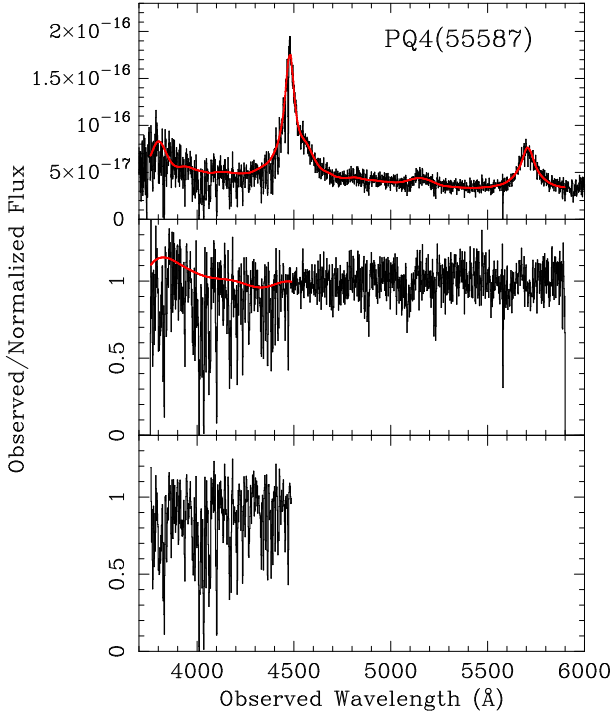


Figure 2. Normalization procedure for the SDSS spectrum (MJD:55587) of a b/g quasar of PQ4 as an example. Top panel: PCA-fit (red curve) to the observed spectrum (black histogram). Middle panel: fit model by a low-order spline function (red curve) to the PCA-normalized spectrum (black histogram). Bottom panel: final normalized spectrum whose transmitted mean flux is consistent with the expected value by Faucher-Giguère et al. (2008).

redshift from the systemic redshift is small enough and smaller than its own uncertainty by a factor of ~ 5 , we regard the primary redshift in Lyke et al. (2020) as the systemic redshift in this study without any corrections.

3.3. Enhancement of quasar ionizing photon flux

An ionization condition of CGM and IGM around the f/g quasars depends on the total number of hydrogen-ionizing photons emitted by the f/g quasars and a distance from them in addition to the extra galactic ionizing background. We calculate the Lyman continuum luminosity of the f/g quasar at $\lambda_{\text{rest}} = 912\text{\AA}$ in the quasar's rest frame assuming isotropic radiation by

$$L_{\nu}^{912} = F_{\nu}^{912} \times 4\pi D_L^2, \quad (2)$$

where F_{ν}^{912} is the specific flux at $\lambda_{\text{rest}} = 912\text{\AA}$ and D_L is the luminosity distance of the f/g quasar, using the same prescription as described in Jalan et al. (2019). The value of F_{ν}^{912} is estimated from the observed flux at $\lambda_{\text{obs}} \sim 1325 \times (1+z_{\text{f/g}})\text{\AA}$, and extrapolated to $\lambda_{\text{rest}} = 912\text{\AA}$ by using a broken power-law (Khaire & Srianand

2015) with a power-law index of $\alpha = 0.44$ (Vanden Berk et al. 2001) at $\lambda_{\text{rest}} > 1300\text{\AA}$ and 1.57 (Telfer et al. 2002) at $\lambda_{\text{rest}} < 1300\text{\AA}$. If we instead use the latest quasar spectral energy distribution (SED) with $\alpha = 0.61$ (Lusso et al. 2015) at $\lambda_{\text{rest}} > 912\text{\AA}$, F_{ν}^{912} and L_{ν}^{912} become larger by a factor of ~ 1.4 . Throughout the paper, we use the original SED above matching to those used in Prochaska et al. (2013) and Jalan et al. (2019).

We also calculate the shortest distance between the f/g quasar and the sight-line toward the b/g quasar by

$$R_{\perp} = D_A \times \theta, \quad (3)$$

where D_A is the angular diameter distance of the f/g quasar and θ is the observed angular separation between the f/g and b/g quasars. We confirm that our sample is not biased, since the distributions of L_{ν}^{912} and R_{\perp} of our BAL quasars are similar to those of non-BAL quasars used in Prochaska et al. (2013) and Jalan et al. (2019), as shown in Figure 5,

Using L_{ν}^{912} and R_{\perp} above, we calculate the enhancement of the quasar ionizing photon flux (F_{qso}) over that of the extragalactic ionizing background (F_{uvb}) at a distance of R_{\perp} by,

$$g_{\text{UV}} = \frac{F_{\text{qso}} + F_{\text{uvb}}}{F_{\text{uvb}}}, \quad (4)$$

assuming the quasar emission is isotropic. Hennawi et al. (2006) calculated g_{UV} assuming a power-law index of $\alpha = 1.8$ in $J_{\nu} \propto \nu^{-\alpha}$ for the mean specific intensity of the extragalactic ionizing background. In this study, we also calculate the enhancement of the ionizing flux using the spectral energy distribution (SED) of J_{ν} as computed by Haardt & Madau (2012) (g_{UV}' , hereafter) in addition to the original one, g_{UV} .

Here, we should note that the photoionization rate depends not only on the ionizing photon flux, but on the H I photoionization cross section that is inversely proportional to the cube of frequency (i.e., $\sigma_{\text{HI}}(\nu) \propto \nu^{-3}$). Therefore, we calculate the H I ionization rates by the quasar's ionizing photon flux (Γ_{qso}) and that due to the extragalactic background ionizing photon flux (Γ_{uvb}). The enhancement of the Γ_{qso} over the Γ_{uvb} at a distance of R_{\perp} is defined as

$$1 + \omega_r = \frac{\Gamma_{\text{uvb}} + \Gamma_{\text{qso}}}{\Gamma_{\text{uvb}}}. \quad (5)$$

The values of g_{UV} and g_{UV}' are slightly different from each other, depending on the SED of the extragalactic background ionizing flux that we assume. On the other hand, the value of $1 + \omega_r$ is almost independent of the SED. So, we will use $1 + \omega_r$ (instead of g_{UV}) for discussing the influence from the quasar's ionizing radiation. The

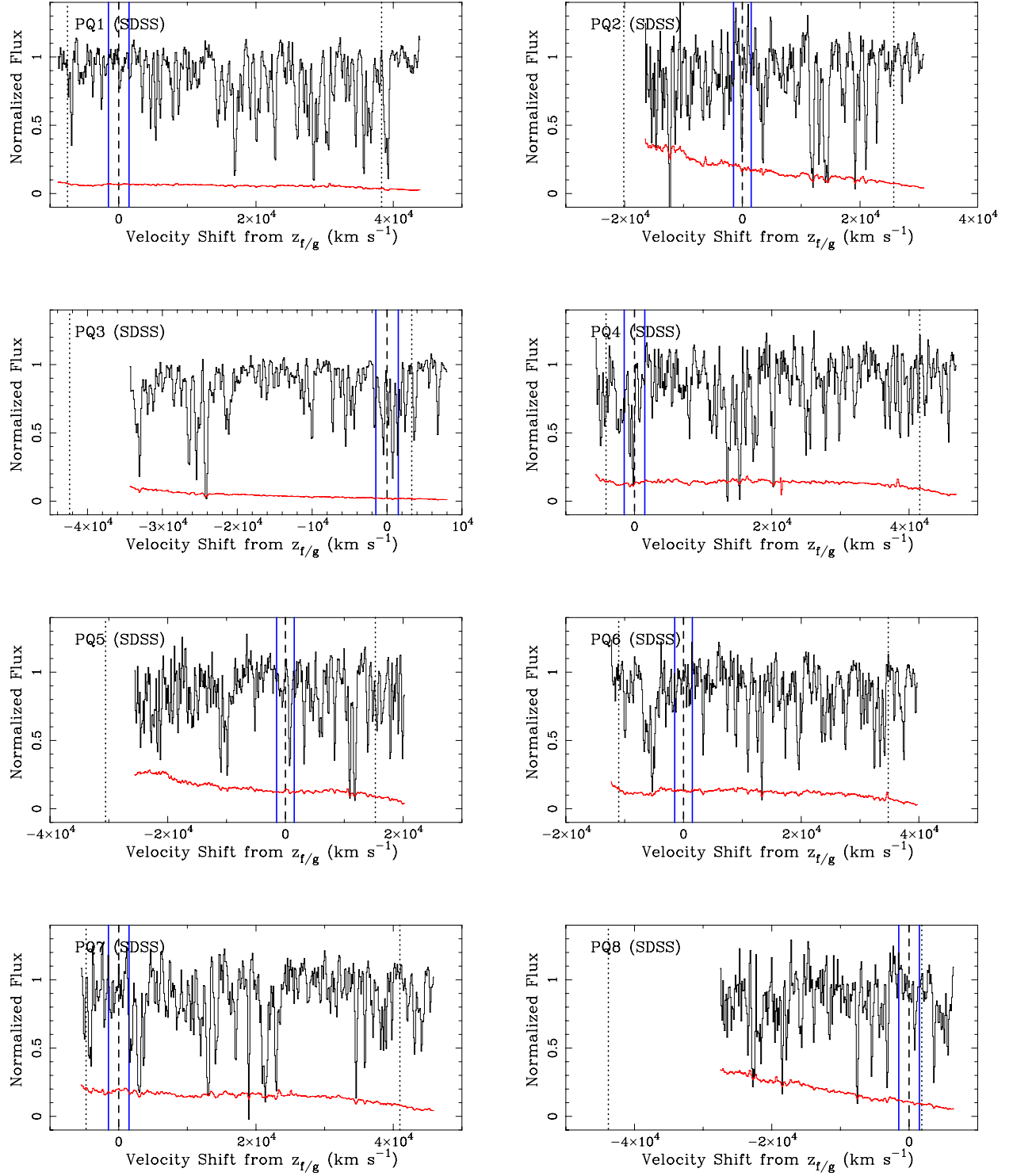


Figure 3. Normalized spectrum as a function of relative velocity from the redshift of f/g quasars as shown with a dashed vertical line. Blue solid vertical lines are $\pm 15,000 \text{ km s}^{-1}$ from $z_{f/g}$. Dotted vertical lines are the lower and upper limits of the optical depth analysis that correspond to Ly β emission (left) and $5,000 \text{ km s}^{-1}$ from $z_{b/g}$ (right).

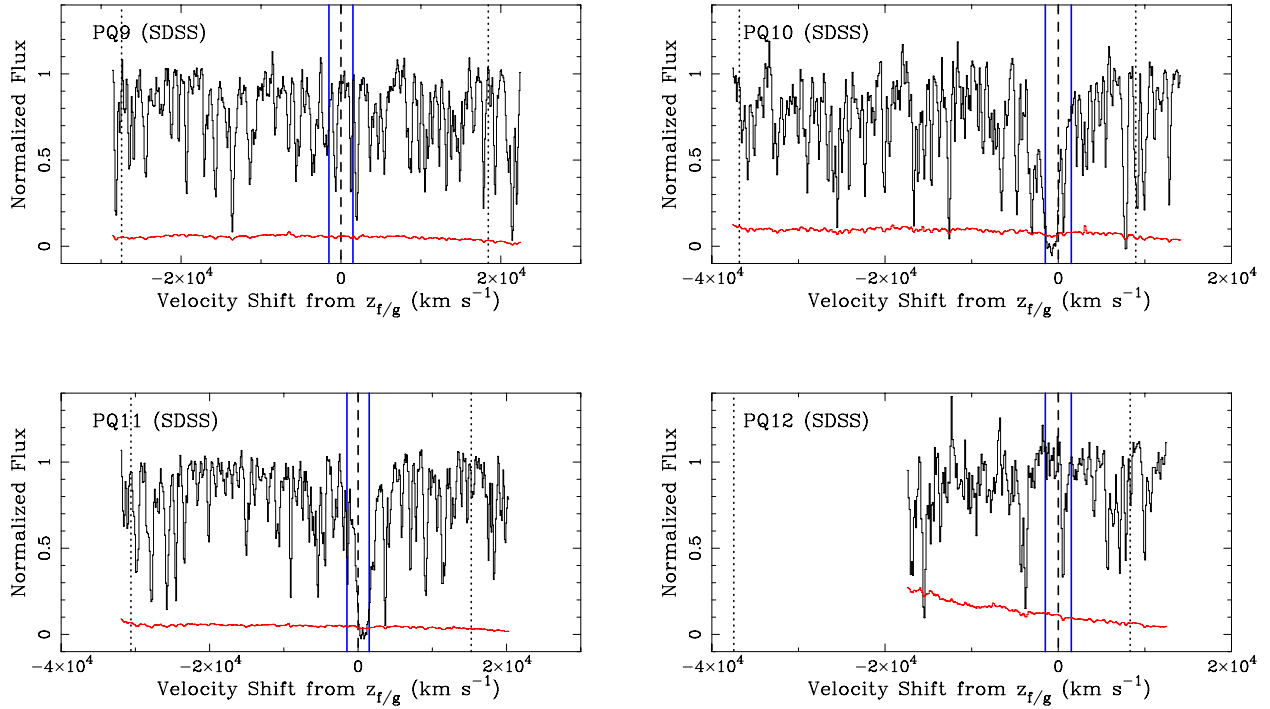


Figure 3. Continued.

values of parameters we calculated are summarized in Table 3.

4. RESULTS

In this section, we examine the H I absorption strength in transverse direction through three analyses following Prochaska et al. (2013): i) measuring the detection rate (i.e., covering fraction, C_f) of optically thick absorbers around BAL quasars, ii) studying how the H I column density at $z_{\text{abs}} \sim z_{f/g}$ correlates with other parameters, iii) examining the H I absorption strength at $z_{\text{abs}} \sim z_{f/g}$ in the stacked spectrum of the b/g quasars.

4.1. Detection Rate of Optically Thick H I Absorbers

Since systemic redshifts that are measured based on Mg II emission lines have their own typical uncertainties with δv of $\sim 300 \text{ km s}^{-1}$, the positions of H I absorption lines corresponding to the CGM and IGM around f/g quasars can be shifted accordingly. The halo gas of f/g quasar also has its own peculiar motion. Therefore, we assume the *strongest* absorption line in $\pm 1500 \text{ km s}^{-1}$ of $z_{f/g}$ as the systems corresponding to the CGM/IGM around f/g quasars following Prochaska et al. (2013). We also measure their column densities using the Voigt profile fitter `mc2fit` (Ishita et al. 2021) with absorption

redshift, column density, and Doppler parameter as free parameters. The relative velocity of the strongest H I line from $z_{f/g}$ and their column density are summarized in Table 3.

As already reported in Lyke et al. (2020), we confirmed there exist candidates of DLA systems with column densities of $\log N_{\text{HI}}/(\text{cm}^{-2}) \gtrsim 20$ in spectra of b/g quasars of PQ10 and PQ11 as shown in Figure 6. Although these systems show damping wings, they could be modeled with multiple weaker components since their line profiles are not continuously saturated at line centers, especially for the system in PQ11. Indeed, a line blending in low-resolution spectrum tends to overestimate the column density. We could not examine the existence of Lyman limits either (i.e., a reliable indicator of DLA systems) since they are outside of our SDSS and FOCAS spectra. However, we detected several low-ionized metal absorption lines (e.g., O II 302, C II 1335, Si II 1260, Si II 1527, and Si IV 1394, 1403) at the redshift of these systems, which suggests that they are closely related to galaxies. Thus, we are not confident that our measured values of $\log N_{\text{HI}}$ are absolutely correct, but their large equivalent widths of $\text{EW}_{\text{rest}} > 10 \text{ \AA}$ (which corresponds to $\log N_{\text{HI}}/(\text{cm}^{-2}) > 20$ at the square-root part of the curve of growth) and the existence of metal absorption lines suggest that their optical depths are at

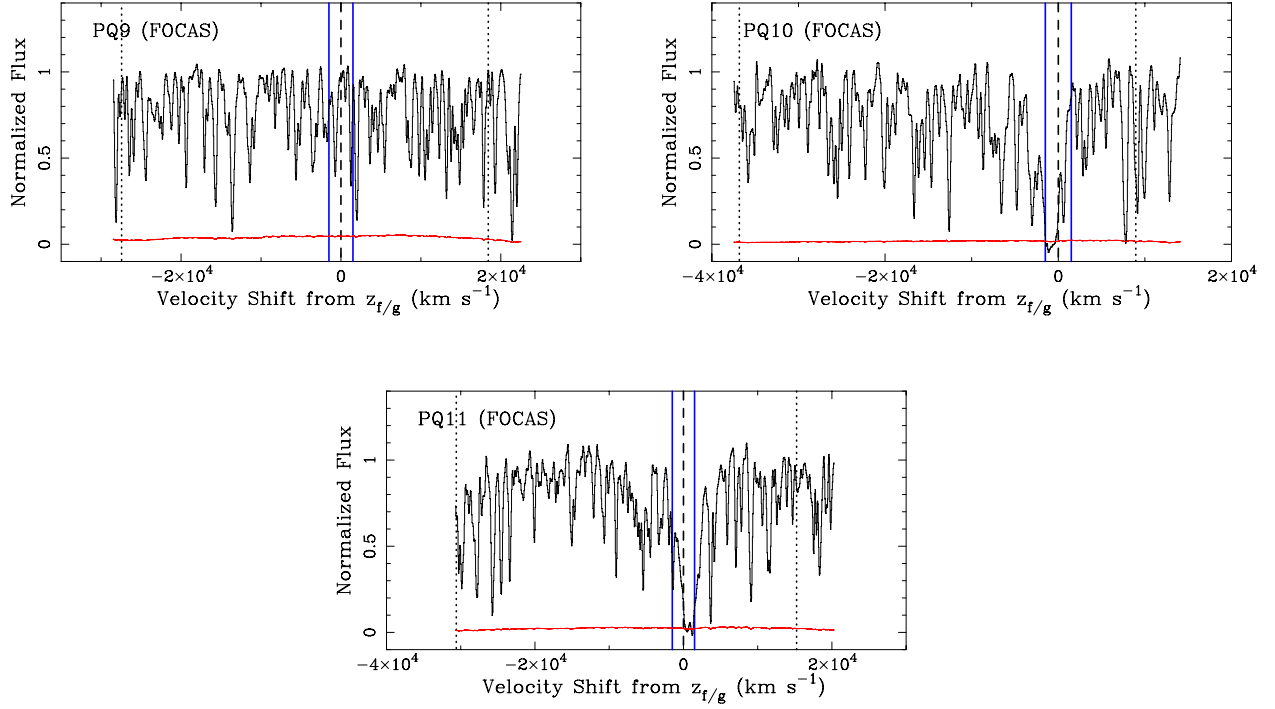


Figure 4. Same as Figure 3, but for PQ9, PQ10, and PQ11 spectra taken with Subaru/FOCAS.

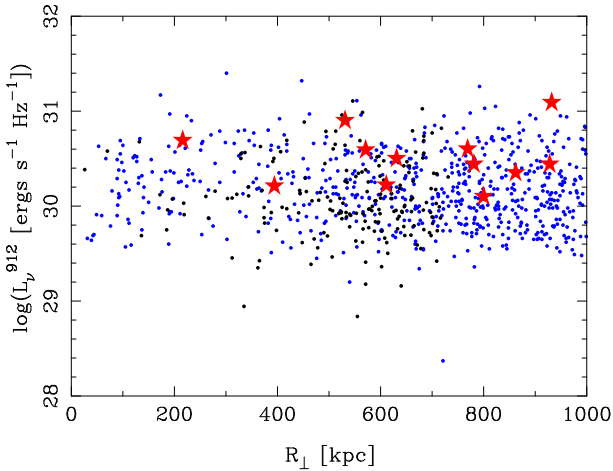


Figure 5. Scatter plot of the Lyman continuum luminosity of the f/g quasars at $\lambda_{\text{rest}} = 912\text{\AA}$ (L_{ν}^{912}) and the perpendicular distance between the f/g quasar and the sight-line toward the b/g quasar (R_{\perp}). Red filled stars are BAL quasars in our sample, while blue and black dots are non-BAL quasars from Prochaska et al. (2013) and Jalan et al. (2019), respectively.

least larger than those of the optically thick absorbers around non-BAL quasars (Prochaska et al. 2013) with

$\text{EW}_{\text{rest}} \sim 1\text{--}2\text{\AA}$ (which corresponds to $\log N_{\text{HI}}/(\text{cm}^{-2}) \gtrsim 17$ at the flat part of the curve of growth).

Thus, the detection rate (i.e., the covering fraction) of optically thick gas around BAL quasars is $C_f = 2/12 \sim 0.17^{+0.22}_{-0.11}$ at $R_{\perp} \sim 220 - 930$ kpc, assuming Poisson noise (Gehrels 1986). Although our C_f estimate has a large uncertainty due to the small sample size, the fraction is consistent to the value estimated at similar transverse distance and velocity interval from non-BAL quasars ($C_f \sim 0.19 \pm 0.02$; Prochaska et al. 2013). We will discuss a large difference in the typical column density of H I absorbers around BAL and non-BAL quasars in Section 5.3.

4.2. Correlations among TPE parameters

Figure 7 summarizes the column density of the strongest H I line in ± 1500 km s $^{-1}$ of $z_{f/g}$ as functions of redshift of foreground quasar ($z_{f/g}$), the transverse distance (R_{\perp}), the enhancement of the ionization rate due to quasar’s ionizing photons ($1+\omega_r$), and the enhancement of the quasar ionizing flux radiation (g_{UV}). As described above, only two b/g quasars (i.e., PQ10 and PQ11) among 12 have absorption systems arising in optically thick absorbers, while the others have only

Table 3. Parameters of Transverse Proximity Effect

ID	$\log L_\nu^{912}(\text{f/g})^a$ (erg/s)	R_\perp^b (kpc)	g_{UV}^c	g'_{UV}^d	$(1 + \omega_r)^e$	Δv^f (km s $^{-1}$)	$\log N_{\text{HI}}^g$ (cm $^{-2}$)	DLA h
PQ1	30.90	531	263.8	61.3	54.8	190	$13.88^{+0.11}_{-0.12}$	
PQ2	30.69	216	995.1	228.7	205.0	−86	$14.43^{+0.13}_{-0.14}$	
PQ3	30.35	862	29.0	7.4	6.7	750	$14.61^{+0.01}_{-0.01}$	
PQ4	30.22	611	43.0	10.6	9.6	−168	$14.63^{+0.12}_{-0.11}$	
PQ5	30.21	394	99.5	23.6	21.2	747	$14.52^{+0.07}_{-0.07}$	
PQ6	30.44	781	44.0	10.9	9.8	−1296	$13.84^{+0.24}_{-0.43}$	
PQ7	30.50	631	75.6	18.1	16.3	−1111	$13.89^{+0.30}_{-0.78}$	
PQ8	31.09	932	133.2	31.4	28.1	835	$14.26^{+0.09}_{-0.09}$	
PQ9	30.59	571	120.4	28.7	25.2	1269 (1249)	$14.35^{+0.02}_{-0.02}$	
PQ10	30.60	769	66.0	16.0	14.2	−829 (−839)	$20.62^{+0.01}_{-0.01}$	$z_{\text{DLA}} = 2.539$
PQ11	30.44	928	31.4	8.0	7.2	746 (768)	$20.75^{+0.00}_{-0.00}$	$z_{\text{DLA}} = 2.443$
PQ12	30.10	800	19.3	5.2	4.7	561	$14.44^{+0.06}_{-0.06}$	

^aSpecific luminosity at $\lambda_{\text{rest}} = 912\text{\AA}$.

^bShortest distance between the f/g quasar and the sightline toward the b/g quasar.

^cEnhancement of the quasar’s ionizing photon flux over that of the extragalactic ionizing background at a distance of R_\perp from foreground quasar, assuming $J_\nu \propto \nu^{-1.8}$ as an SED of the extragalactic ionizing background (Hennawi et al. 2006).

^dSame as g_{UV} , but using the version of J_ν computed by Haardt & Madau (2012) for the extragalactic ionizing background.

^eEnhancement of the H I ionization rate including the quasar’s ionizing photon over that due to only the extragalactic ionizing background at a distance of R_\perp from a foreground quasar, using the version of J_ν computed by Haardt & Madau (2012) for the extragalactic ionizing background.

^fRelative velocity between $z_{\text{f/g}}$ and z_{abs} of the strongest H I line in ± 1500 km s $^{-1}$ of $z_{\text{f/g}}$. Numbers in parentheses are measured in FOCAS spectra.

^gH I column density of the strongest absorption line in ± 1500 km s $^{-1}$ of $z_{\text{f/g}}$, which are measured in FOCAS spectra for PQ9, PQ10, and PQ11 and SDSS spectra for the other quasars.

^hRedshift of Damped Ly α system detected in ± 1500 km s $^{-1}$ of $z_{\text{f/g}}$, as discovered by Lyke et al. (2020).

weaker lines with column densities of $\log N_{\text{HI}}/(\text{cm}^{-2}) < 15$. Thus, there is a large gap (about five orders of magnitude) in the column densities of the strongest H I absorbers in the b/g quasar’s spectra of PQ10 and PQ11 and those of the other 10 quasars. Possible origins of the large column densities in the former quasars includes i) there exist over density regions that is exposed to the same level of ionizing radiation as those around the other f/g quasars and ii) there exist normal CGM/IGM absorbers but less illuminated by f/g quasars. However, the second scenario is immediately rejected, since the enhancement of the H I ionization rate ($1 + \omega_r$) of PQ10 and PQ11 (14.2 and 7.2) is comparable to those around the other quasar pairs. Moreover, we do not find any

correlations of $\log N_{\text{HI}}$ as functions of R_\perp and $(1 + \omega_r)$, as seen in the second and third panels from the left in Figure 7, though the statistical significance is not so high due to the small sample size. Only PQ2 has an ionization enhancement ($(1 + \omega_r) = 205$) larger than 100, and much larger than the other quasar pairs by almost one order of magnitude, but its H I column density is comparable to the others. It should be noted that two f/g quasars (i.e., PQ10 and PQ11) with optically thick absorbers around them tend to have larger redshift ($z_{\text{f/g}} > 2.4$). We will discuss these in Section 5.2.

4.3. Stacked Spectrum

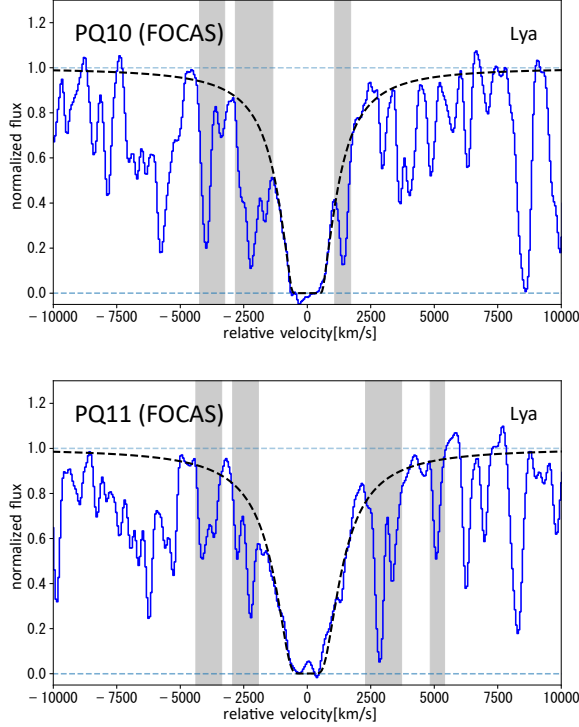


Figure 6. Observed spectrum (blue histogram) and best fit model (black dashed curve) of strong H I absorption lines at $z_{\text{abs}} \sim z_{\text{f/g}}$ in b/g quasars of PQ10 (top) and PQ11 (bottom). Shaded areas are ignored while model fitting due to blending with other lines.

It is not easy to detect H I absorption lines corresponding to the CGM/IGM around the f/g quasars, since they are severely blended with Ly α forest arising in cosmologically distributed IGM. Therefore, we create the composite spectra of the 12 b/g quasars as a function of relative velocity or radial distance (assuming Hubble flow) from $z_{\text{f/g}}$, to increase S/N ratio in the stacked spectrum and to suppress the contamination by unrelated Ly α forest. The spectra combined by average and median values are shown in Figure 8. After normalizing their flux levels by those expected from the IGM (Faucher-Giguère et al. 2008), we measure EW_{rest} of Ly α absorption directly from the stacked spectra in $\pm 1500 \text{ km s}^{-1}$ of the center without applying Gaussian fit. We marginally detect a weak absorption profile in the mean stack spectrum with $\text{EW}_{\text{rest}} = 0.97 \pm 0.26 \text{ \AA}$ (which is consistent to the expected value ($\text{EW}_{\text{rest}} = 0.99 \pm 0.17 \text{ \AA}$) from those around non-BAL quasars (Prochaska et al. 2013), as compared in Figure 9). However, the mean stack spectrum is biased significantly due to the existence of the two DLA systems. Therefore, we also measure EW_{rest} in the median stack spectrum and acquire $\text{EW}_{\text{rest}} < 0.28 \text{ \AA}$. We

will consider the former and the latter as the upper and lower limits of EW_{rest} .

We also create composite spectra, using only nine and three b/g quasars whose corresponding f/g quasars are at $z_{\text{f/g}} < 2.3$ and > 2.4 , since f/g quasars with optically thick absorbers (i.e., DLA systems) are detected only at $z > 2.4$. We do not detect any remarkable absorption troughs in the combined spectrum of 9 quasars at lower redshift. On the other hand, there exists a broad ($\geq 2000 \text{ km s}^{-1}$) and strong absorption feature in the combined spectra of 3 quasars at higher redshift, since two of the three quasars have optically thick absorption lines as described in Section 4.1. We also create the same stacked spectra after setting centers of the strongest H I absorption lines as the system centers (Figure 10). In this case, we detect narrow and deep lines at the centers in both mean and median spectra combining all 12 quasars and 9 quasars at lower redshift. In the combined spectrum of 3 higher- z quasars, we detect strong H I absorption lines again, but their profiles are deeper and smoother.

5. DISCUSSION

In this study, we examine the strength of H I absorption lines arising in the CGM/IGM around BAL quasars in an impact parameter of $\lesssim 1 \text{ Mpc}$. We detect optically thick absorbers around two out of 12 BAL quasars whose detection rate is consistent to the past results around non-BAL quasars (Hennawi et al. 2006; Prochaska et al. 2013). In the mean stack spectrum of 12 BAL quasars, we detect a weak H I absorption line whose strength is also comparable to that around non-BAL quasars. However, the statistical confidence in these results is not very high due to the small sample size. The column densities of optically thick H I absorbers around BAL (this study) and non-BAL quasars (Prochaska et al. 2013) also have a large difference by about three orders of magnitude. In this section, we first discuss if BAL quasars can be used as an indicator that they are observed from a direction close to the side. We then consider a possible redshift evolution of BAL quasars, and finally discuss possible origins of anisotropy of the proximity effect (between LPE and TPE) around quasars.

5.1. Inclination Scenario of BAL Quasars

The dust torus, an essential structure for the AGN unification model, has been considered as an origin of the anisotropic H I absorption around quasars (Prochaska et al. 2013; Jalan et al. 2019) through shielding effect of ionizing photon flux radiation from the continuum source. If this is the case, we expect a small amount of neutral Hydrogen in the direction with small

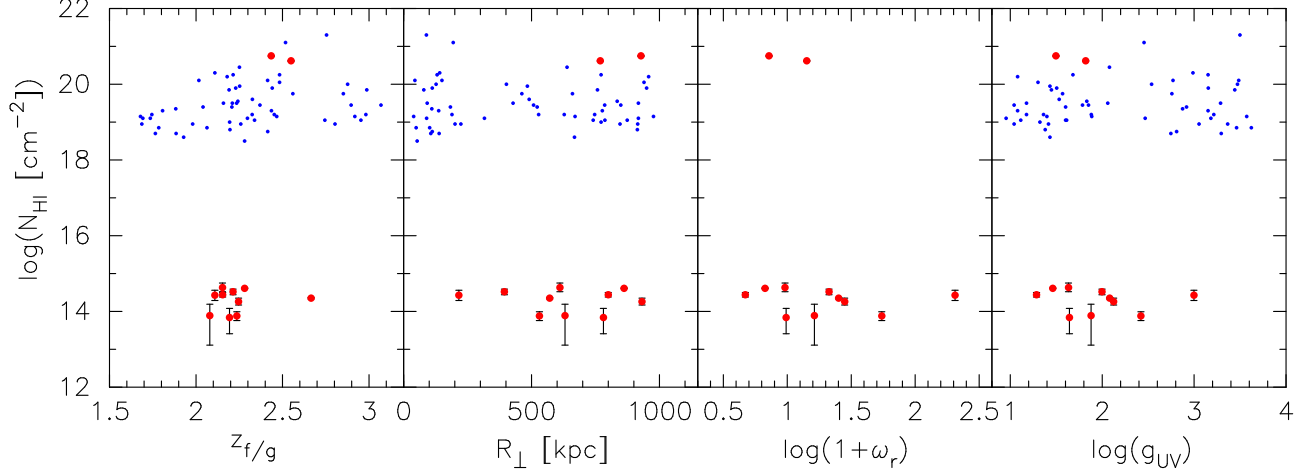


Figure 7. Column density distribution of the strongest H I absorption line in $\pm 1500 \text{ km s}^{-1}$ of $z_{f/g}$ as functions of redshift of foreground quasar ($z_{f/g}$), transverse distance between f/g quasars and lines of sight to b/g quasars (R_{\perp}), enhancement of the H I ionization rate ($1+\omega_r$) and the H I ionization radiation flux (g_{UV}) due to the quasar's ionizing photon over that due to only the extragalactic ionization background at R_{\perp} . Filled red circles denote BAL quasars (this study), while blue dots are optically thick absorbers around non-BAL quasars (Prochaska et al. 2013). Note that more than 80% of quasars in Prochaska et al. (2013) are not plotted here, since only upper limits of $\log N_{\text{HI}}$ are placed due to their low S/N spectra.

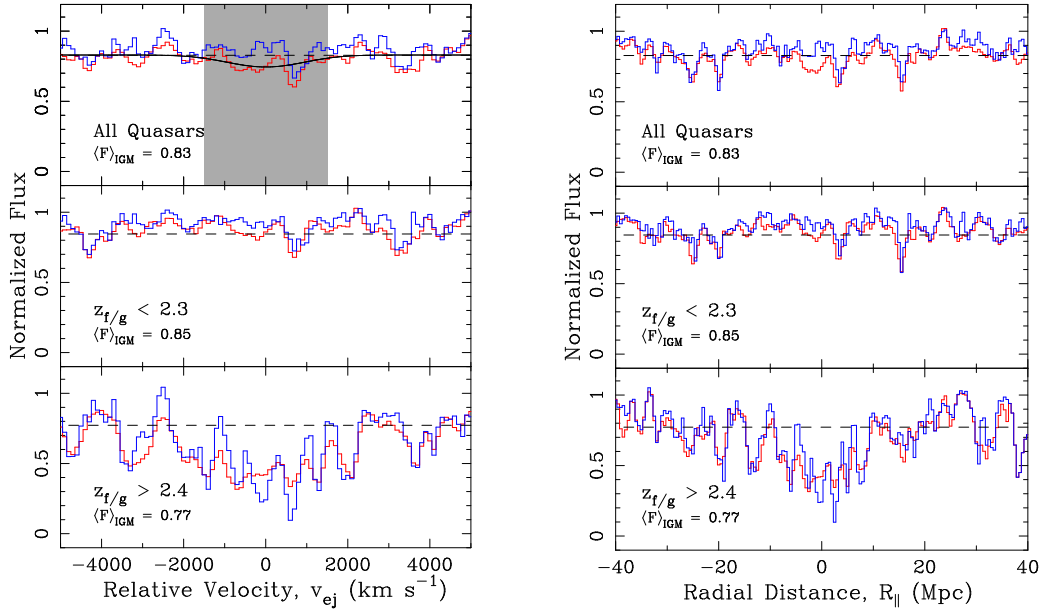


Figure 8. Mean (red) and median (blue) spectra of quasars as a function of relative velocity (left) or radial distance (right) from $z_{f/g}$. Top panel includes all 12 quasars, while middle and bottom panels contain only 9 and 3 quasars whose f/g quasars at $z_{f/g} < 2.3$ or $z_{f/g} > 2.4$. Horizontal dashed lines denote the mean flux of the IGM estimated by Faucher-Giguère et al. (2008). Solid black curve in a top panel of left figure is the mean absorption profile around non-BAL quasars with $\text{EW}_{\text{rest}} = 0.99 \text{ \AA}$ and the velocity dispersion of $\sigma = 917 \text{ km s}^{-1}$ at similar perpendicular distance (Prochaska et al. 2013). Shaded area in the same panel denotes the velocity range (i.e., $\pm 1500 \text{ km s}^{-1}$) at which EW_{rest} is measured for our stacked spectra.

inclination angles (i.e., close to the face-on direction from the accretion disk) since they are not shielded by the dust torus. It is widely believed that BAL profiles are observed if we observe the continuum source from near the side since the AGN outflow wind (i.e., BAL

absorber) are accelerated in a direction with larger inclination angles (e.g., Murray et al. 1995; Proga et al. 2000). For example, Elvis (2000) proposes a funnel-shaped thin outflow wind as a BAL absorber with a cone angle of ~ 60 degree to the accretion disk axis. Thus,

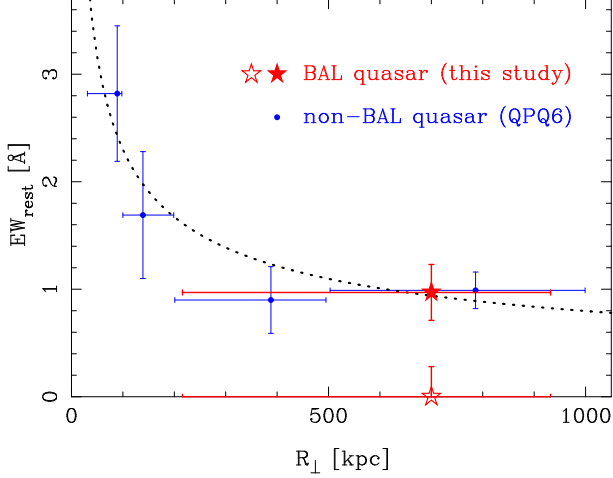


Figure 9. Rest-frame equivalent width as a function of the transverse distance from f/g quasar. Red filled and open stars with error bars are equivalent widths of H I absorption profile in the mean and median stack spectra of our 12 BAL quasars, which denote upper and lower limits of EW_{rest} . The horizontal error is the distribution of R_{\perp} of the 12 quasar pairs, while the vertical error is the statistical uncertainty of EW_{rest} assuming the S/N ratio of the combined spectra (~ 8 per pixel). Blue dots with error bars denote EW_{rest} of non-BAL quasars (Prochaska et al. 2013). Black dotted curve is a fitted model of non-BAL quasars that was introduced by Prochaska et al. (2013) as $EW_{\text{rest}} = 2.3 \times (R_{\perp}/100 \text{ kpc})^{-0.46} \text{ \AA}$.

positive (i.e., more ionized) transverse proximity effect is expected around BAL quasars, while *negative* (i.e., less ionized) TPE was observed around non-BAL quasars.

Contrary to the expectations above, we found that the detection rate of optically thick absorbers around BAL quasars in the transverse direction is at the same level as that seen around non-BAL quasars ($C_f \sim 0.2$). If we consider only DLAs with $\log N_{\text{HI}}/(\text{cm}^{-2}) \gtrsim 20$, the detection rate is even larger around BAL quasars ($C_f = 0.17^{+0.22}_{-0.11}$) than that around non-BAL quasars ($C_f = 0.02 \pm 0.01$; Prochaska et al. 2013). The absorption strength (i.e., equivalent width) of H I absorption trough in the mean stack spectrum of all 12 BAL quasars is also consistent to the value that is expected from non-BAL quasars (see Figure 9). These results seem to suggest that BAL quasars may not be a good indicator that they are observed from a direction close to the dust torus. Even if the inclination angles of BAL quasars are indeed large, the dust torus around them may not be a dominant source of the anisotropic proximity effect. Recently, Giustini & Proga (2019) propose a global view of AGN accretion disk winds, in which the outflow winds have smaller inclination angle relative to the rotation axis with increasing Eddington ratio, and

that they eventually become almost polar-winds in the case of super-Eddington. Thus, if this is the case, we need other parameters of quasars such as Eddington ratio and black hole mass in addition to the existence of BAL profiles, to examine the effect of the inclination angle of quasars more precisely.

On the other hand, if we remove DLA systems from our sample, the detection rate of optically thick absorbers would be $C_f = 0/10 \sim 0^{+0.18}_{-0}$. The H I absorption strength in the median stack spectrum also becomes smaller ($EW_{\text{rest}} < 0.28 \text{ \AA}$). Although the confidence level is not very high, both of them are smaller than those around non-BAL quasars, which is consistent with the anisotropic scenario due to the dust torus. We will discuss a possible origin of DLA systems around BAL quasars in Section 5.3.

5.2. Redshift Evolution of BAL Quasars

As noted in Section 4.2, DLAs are detected only around BAL quasars at higher redshift ($z_{f/g} > 2.4$) in our sample. If we consider only 3 BAL quasars at $z_{f/g} > 2.4$, the detection rate of DLA absorber is quite large ($C_f = 0.67^{+0.33}_{-0.43}$), while the detection rate is very small ($C_f = 0^{+0.21}_{-0}$) at $z_{f/g} < 2.4$. On the other hand, around *non-BAL* quasars, we do not find any differences between the detection rates at $z_{f/g} > 2.4$ ($C_f = 0.02 \pm 0.01$) and at $z_{f/g} < 2.4$ ($C_f = 0.02 \pm 0.01$), using the sample of Prochaska et al. (2013).

The difference between BAL quasars at lower and higher redshift could be related to the evolution effect. For example, the fraction of BAL quasars increases by a factor of ~ 3.5 from $z < 2.3$ to $z > 3.5$, although there is a large uncertainty at $z = 2.3 - 3.0$ (Allen et al. 2011). It is also suggested that quasars with BAL (especially LoBAL) are probably in the early stage of AGN evolution between ultra luminous infrared galaxies (ULIRGs) and normal unobscured quasars, since they have high star formation activity (e.g., Becker et al. 2000; Farrah et al. 2007).

Thus, we speculate that our results could support that BAL quasars evolve with redshift in terms of ionizing photon flux radiation; e.g., BAL quasars at higher redshift have not blown off dust envelope completely and they are still covered by shielding materials with larger covering fraction like LoBAL quasars.

If this is the case, the two BAL quasars with DLA systems around them should be highly reddened by dust envelopes, at least compared to the other 10 BAL quasars without DLAs. To verify this, we perform the spectral fitting for all f/g BAL quasars assuming the same SED as used in Section 3.3 with the extinction law of Calzetti

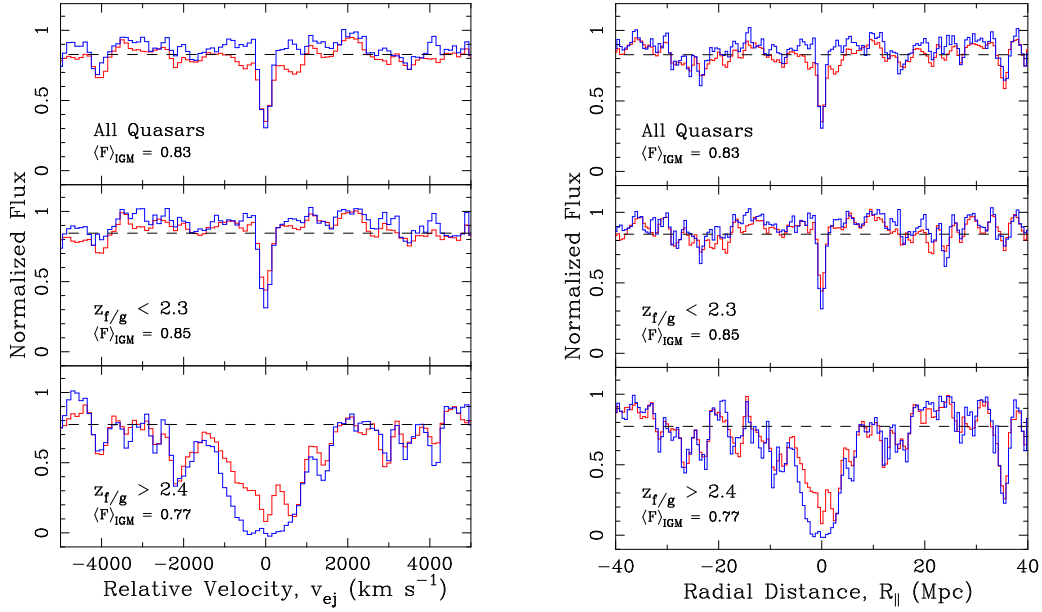


Figure 10. Same as Figure 8, but combined spectra after setting their local absorption peaks in $\pm 1500 \text{ km s}^{-1}$ of $z_{f/g}$ as the system center.

et al. (2000) to estimate the dust reddening.⁹ The average value of the derived intrinsic color excess of the two BAL quasars with DLAs is $E(B - V) = 0.12 \pm 0.11$, while that of the other 10 BAL quasars without DLAs is $E(B - V) = 0.33 \pm 0.25$. Thus, we do not find any obvious trends of more dust around the former quasars. We need to increase the sample size to place more stringent constraints on redshift evolution of BAL quasars at a statistically significant level.

5.3. Anisotropy of Proximity Effect around Quasars

The anisotropic proximity effect cannot be reconciled with an isotropically emitting flux source. In addition to the enhancement of ionizing flux radiation, Jalan et al. (2019, 2021) also considered the gas over-density effect around quasars. They derived the excess over density up to $\sim 5 \text{ Mpc}$ from quasars in the both line-of-sight and transverse directions, but they confirmed that the material in the transverse direction should not be illuminated more than 27% of the radiation level in the line-of-sight direction from the quasars to reconcile the difference (i.e., the anisotropic proximity effect still remains even after considering gas over density.).

There are several interpretations for the anisotropy such as i) an intrinsic anisotropy of the ionizing flux radiation due to structures of host galaxies and/or the

accretion disks, ii) anisotropic obscuration by the dust torus, iii) the finite lifetime of the quasars¹⁰, and iv) the inflow of matter into (or the outflow of the matter from) the halo of quasar host galaxies (e.g., Prochaska et al. 2013; Jalan et al. 2019, and references therein).

In this study, we verified the anisotropic obscuration scenario by the dust torus as the origin of the difference between LPE and TPE. This scenario has been thought to be the most probable one, since the existence of the dust torus has been confirmed by various observations (e.g., Antonucci 1993) and its opening angle is constrained to be large enough (Schirber et al. 2004; Kirkman & Tytler 2008; Lu & Yu 2011). Contrary to the expectation, we detect i) two optically thick DLA-like absorbers and ii) a weak H I absorption in the mean stack spectrum with $\text{EW}_{\text{rest}} \sim 1 \text{ \AA}$ (at the same level as non-BAL quasars) around BAL quasars whose inclination angle is expected to be large (i.e., close to the edge-on along our lines of sight).

However, the column densities of optically thick absorbers differ by about three orders of magnitude between those around BAL quasars (i.e., DLA-like ab-

⁹ Before the fitting, we correct for the Galactic extinction using the Galactic color excess $E(B - V)$ (Schlegel et al. 1998) and the extinction law of Cardelli et al. (1989).

¹⁰ Quasar lifetime is short enough for ionizing photons from the f/g quasars to propagate into the CGM/IGM along the lines of sight to b/g quasars ($t_{\text{qso}} \lesssim 1 \text{ Myr}$). Since a typical scale of LPE and TPE studies is $\sim 1 \text{ Mpc}$ (i.e., millions of light years), the light travel time from the CGM/IGM in the line-of-sight direction (after being sufficiently ionized) is shorter than that from the CGM/IGM in the transverse direction (before being ionized) by a few Myrs.

sorbers with $\log N_{\text{HI}}/(\text{cm}^{-2}) \sim 20$; this study) and non-BAL quasars (i.e., Lyman limit system (LLS)-like absorbers with $\log N_{\text{HI}}/(\text{cm}^{-2}) \gtrsim 17.2$; Prochaska et al. 2013). Indeed, around non-BAL quasars, both the covering fraction ($C_f \sim 0\%$ at $R_\perp \sim 1$ Mpc) and the clustering amplitude ($r_0 \sim 4$ Mpc) of the quasar-absorber cross-correlation function¹¹ of DLAs is very different from those of LLSs ($C_f \sim 20\%$ and $r_0 \sim 19$ Mpc), which suggests that the former traces galaxies within the same dark matter halos as f/g BAL quasars and that the latter arises at a dense, self-shielding media in large-scale structures like filaments (Prochaska et al. 2013). If this is the case, the statistical analyses based on the large sample size of the systems without DLA-like systems would be required to probe the environment around the BAL quasars since the existence of galaxies would bias toward larger column densities. As noted in Section 5.1, the covering fraction of optically thick gas around BAL quasars (after removing DLA-like systems) would be smaller than that around non-BAL quasars although not statistically significant, which is expected from the anisotropic scenario (Prochaska et al. 2013; Jalan et al. 2019).

6. SUMMARY

In this study, we examined environments of BAL quasars whose inclination angle is considered to be large (i.e., we observe them close to the side.). To study H I absorption strength around foreground BAL quasars in spectra of background quasars, we targeted closely separated 12 quasar pairs at different redshift with separation angle of $\theta < 120''$ ($\lesssim 1$ Mpc at $z \sim 2$). We used low-resolution spectra ($R \sim 2000$) of SDSS quasars and those obtained by ourselves with Subaru/FOCAS. Because it is difficult to fit the continuum level directly in the spectral region of Ly α forest, we first roughly estimated the quasar's intrinsic spectra using a PCA method with template spectra of low-redshift quasars. Then, we manually normalized them again with a low-order spline function to satisfy the mean flux of the IGM.

We measured the H I absorption strength in an individual quasar spectrum. We confirmed there exist optically thick gas around two BAL quasars, whose detection rate is consistent to the past results around non-BAL quasars. We also created the composite mean spectrum of all 12 background quasars and marginally detected a weak absorption profile at $z_{\text{f/g}}$, whose absorption strength is consistent with the expected value from those around non-BAL quasars.

We also confirmed that only high redshift BAL quasars at $z_{\text{f/g}} > 2.4$ have the corresponding optically thick gas, which implies a possible redshift evolution of BAL quasars. However, we do not find any obvious trends of more dust around higher redshift BAL quasars based on our relatively small sample size.

Taking the results above into account, the anisotropic obscuration due to the dust torus cannot reconcile the difference in the H I absorption strength around quasars by itself. However, these results are not statistically significant due to the small sample size. Moreover, if we remove DLAs (whose origin is probably different from those of LLSs) from our sample, both the covering fraction and the mean absorption strength of optically thick gas around BAL quasars would be smaller than that around non-BAL quasars, which still supports the anisotropic scenario.

There are other possible ideas for the anisotropic proximity effect. For example, the quasars may have a finite lifetime and their ionizing photons have not reached to the CGM/IGM in the transverse direction. Another possibility is that the two BAL quasars with DLA systems (i.e., PQ10 and PQ11) have smaller inclination angle than those of the other BAL quasars so that the CGM/IGM in the transverse direction are less ionized like those around non-BAL quasars.

For narrowing down possible scenarios further, we plan to increase the sample size significantly by searching for fainter quasar pairs that satisfy all the criteria except for g -band magnitude in Section 2.1, using Prime Focus Spectrograph that will be installed to Subaru telescope soon.

¹¹ $\xi_{\text{QA}}(r) = (r/r_0)^{-\gamma}$, where $\gamma = 1.6$, assuming galaxy-galaxy clustering (Adelberger et al. 2005).

We thank the anonymous referee for very useful comments and suggestions. This research is based in part on data collected at the Subaru Telescope, which is operated by the National Astronomical Observatory of Japan. We are honored and grateful for the opportunity of observing the Universe from Maunakea, which has the cultural, historical, and natural significance in Hawaii. This work was supported by JSPS KAKENHI Grant Number 21H01126.

Funding for the Sloan Digital Sky Survey IV has been provided by the Alfred P. Sloan Foundation, the U.S. Department of Energy Office of Science, and the Participating Institutions. SDSS-IV acknowledges support and resources from the Center for High Performance Computing at the University of Utah. The SDSS website is www.sdss.org.

SDSS-IV is managed by the Astrophysical Research Consortium for the Participating Institutions of the SDSS Collaboration including the Brazilian Participation Group, the Carnegie Institution for Science, Carnegie Mellon University, Center for Astrophysics — Harvard & Smithsonian, the Chilean Participation Group, the French Participation Group, Instituto de Astrofísica de Canarias, The Johns Hopkins University, Kavli Institute for the Physics and Mathematics of the Universe (IPMU) / University of Tokyo, the Korean Participation Group, Lawrence Berkeley National Laboratory, Leibniz Institut für Astrophysik Potsdam (AIP), Max-Planck-Institut für Astronomie (MPIA Heidelberg), Max-Planck-Institut für Astrophysik (MPA Garching), Max-Planck-Institut für Extraterrestrische Physik (MPE), National Astronomical Observatories of China, New Mexico State University, New York University, University of Notre Dame, Observatório Nacional / MCTI, The Ohio State University, Pennsylvania State University, Shanghai Astronomical Observatory, United Kingdom Participation Group, Universidad Nacional Autónoma de México, University of Arizona, University of Colorado Boulder, University of Oxford, University of Portsmouth, University of Utah, University of Virginia, University of Washington, University of Wisconsin, Vanderbilt University, and Yale University.

REFERENCES

- Adelberger, K. L., Steidel, C. C., Pettini, M., et al. 2005, *ApJ*, 619, 697. doi:10.1086/426580
- Allen, J. T., Hewett, P. C., Maddox, N., et al. 2011, *MNRAS*, 410, 860. doi:10.1111/j.1365-2966.2010.17489.x
- Antonucci, R. 1993, *ARA&A*, 31, 473. doi:10.1146/annurev.aa.31.090193.002353
- Bajtlik, S., Duncan, R. C., & Ostriker, J. P. 1988, *ApJ*, 327, 570. doi:10.1086/166217
- Becker, R. H., White, R. L., Gregg, M. D., et al. 2000, *ApJ*, 538, 72. doi:10.1086/309099
- Cardelli, J. A., Clayton, G. C., & Mathis, J. S. 1989, *ApJ*, 345, 245. doi:10.1086/167900
- Calzetti, D., Armus, L., Bohlin, R. C., et al. 2000, *ApJ*, 533, 682. doi:10.1086/308692
- Chen, Z., He, Z., Ho, L. C., et al. 2022, *Nature Astronomy*, 6, 339. doi:10.1038/s41550-021-01561-3
- Croft, R. A. C. 2004, *ApJ*, 610, 642. doi:10.1086/421839
- Elvis, M. 2000, *ApJ*, 545, 63. doi:10.1086/317778
- Farrah, D., Lacy, M., Priddey, R., et al. 2007, *ApJL*, 662, L59. doi:10.1086/519492
- Faucher-Giguère, C.-A., Prochaska, J. X., Lidz, A., et al. 2008, *ApJ*, 681, 831. doi:10.1086/588648
- Filiz Ak, N., Brandt, W. N., Hall, P. B., et al. 2013, *ApJ*, 777, 168. doi:10.1088/0004-637X/777/2/168
- Gehrels, N. 1986, *ApJ*, 303, 336. doi:10.1086/164079
- Giustini, M. & Proga, D. 2019, *A&A*, 630, A94. doi:10.1051/0004-6361/201833810
- Haardt, F. & Madau, P. 2012, *ApJ*, 746, 125. doi:10.1088/0004-637X/746/2/125
- Hall, P. B., Anderson, S. F., Strauss, M. A., et al. 2002, *ApJS*, 141, 267. doi:10.1086/340546
- Hennawi, J. F., Prochaska, J. X., Burles, S., et al. 2006, *ApJ*, 651, 61. doi:10.1086/507069
- Hennawi, J. F. & Prochaska, J. X. 2013, *ApJ*, 766, 58. doi:10.1088/0004-637X/766/1/58
- Ishimoto, R., Kashikawa, N., Onoue, M., et al. 2020, *ApJ*, 903, 60. doi:10.3847/1538-4357/abb80b
- Ishita, D., Misawa, T., Itoh, D., et al. 2021, *ApJ*, 921, 119. doi:10.3847/1538-4357/ac14b4
- Jalan, P., Chand, H., & Srianand, R. 2019, *ApJ*, 884, 151. doi:10.3847/1538-4357/ab4191
- Jalan, P., Chand, H., & Srianand, R. 2021, *MNRAS*, 505, 689. doi:10.1093/mnras/stab1303
- Khaire, V. & Srianand, R. 2015, *ApJ*, 805, 33. doi:10.1088/0004-637X/805/1/33
- Kirkman, D. & Tytler, D. 2008, *MNRAS*, 391, 1457. doi:10.1111/j.1365-2966.2008.13994.x
- Knigge, C., Scaringi, S., Goad, M. R., et al. 2008, *MNRAS*, 386, 1426. doi:10.1111/j.1365-2966.2008.13081.x
- Lípari, S. L. & Terlevich, R. J. 2006, *MNRAS*, 368, 1001. doi:10.1111/j.1365-2966.2006.10215.x
- Lu, Y. & Yu, Q. 2011, *ApJ*, 736, 49. doi:10.1088/0004-637X/736/1/49
- Lusso, E., Worseck, G., Hennawi, J. F., et al. 2015, *MNRAS*, 449, 4204. doi:10.1093/mnras/stv516
- Lyke, B. W., Higley, A. N., McLane, J. N., et al. 2020, *ApJS*, 250, 8. doi:10.3847/1538-4365/aba623
- Murray, N., Chiang, J., Grossman, S. A., et al. 1995, *ApJ*, 451, 498. doi:10.1086/176238
- Pâris, I., Petitjean, P., Ross, N. P., et al. 2017, *A&A*, 597, A79. doi:10.1051/0004-6361/201527999
- Pâris, I., Petitjean, P., Rollinde, E., et al. 2011, *A&A*, 530, A50. doi:10.1051/0004-6361/201016233
- Prochaska, J. X., Hennawi, J. F., Lee, K.-G., et al. 2013, *ApJ*, 776, 136. doi:10.1088/0004-637X/776/2/136
- Proga, D., Stone, J. M., & Kallman, T. R. 2000, *ApJ*, 543, 686. doi:10.1086/317154
- Schirber, M., Miralda-Escudé, J., & McDonald, P. 2004, *ApJ*, 610, 105. doi:10.1086/421451
- Schlegel, D. J., Finkbeiner, D. P., & Davis, M. 1998, *ApJ*, 500, 525. doi:10.1086/305772
- Scott, J., Bechtold, J., Dobrzycki, A., et al. 2000, *ApJS*, 130, 67. doi:10.1086/317340
- Shen, Y., Brandt, W. N., Richards, G. T., et al. 2016, *ApJ*, 831, 7. doi:10.3847/0004-637X/831/1/7
- Suzuki, N., Tytler, D., Kirkman, D., et al. 2005, *ApJ*, 618, 592. doi:10.1086/426062
- Telfer, R. C., Zheng, W., Kriss, G. A., et al. 2002, *ApJ*, 565, 773. doi:10.1086/324689
- Treister, E. & Urry, C. M. 2005, *ApJ*, 630, 115. doi:10.1086/431892
- Ueda, Y., Akiyama, M., Ohta, K., et al. 2003, *ApJ*, 598, 886. doi:10.1086/378940
- Urrutia, T., Becker, R. H., White, R. L., et al. 2009, *ApJ*, 698, 1095. doi:10.1088/0004-637X/698/2/1095
- Vanden Berk, D. E., Richards, G. T., Bauer, A., et al. 2001, *AJ*, 122, 549. doi:10.1086/321167
- Weymann, R. J., Morris, S. L., Foltz, C. B., et al. 1991, *ApJ*, 373, 23. doi:10.1086/170020